ASEAN Engineering Journal

Full Paper

DEVELOPMENT OF PEAK GROUND ACCELERATION USING A NON-LINEAR APPROACH TO EVALUATE LIQUEFACTION POTENTIAL IN SEI WAMPU BRIDGE, LANGKAT, NORTH SUMATRA, INDONESIA

Izzatul Aini[a], Wahyu Wilopo[b*], T. Faisal Fathani[c,d]

[a]Natural Disaster Management Engineering, Department of Civil and Environmental Engineering, Universitas Gadjah Mada, Indonesia
[b]Department of Geological Engineering, Universitas Gadjah Mada, Yogyakarta, Indonesia
[c]Department of Civil and Environmental Engineering, Universitas Gadjah Mada, Yogyakarta, Indonesia
[d]Center for Disaster Mitigation and Technological Innovation (GAMA-InaTEK) Universitas Gadjah Mada, Yogyakarta, Indonesia

Article history
Received
18 June 2023
Received in revised form
10 October 2023
Accepted
24 October 2023
Published online
31 August 2024

*Corresponding author
wilopo_w@ugm.ac.id

Graphical abstract

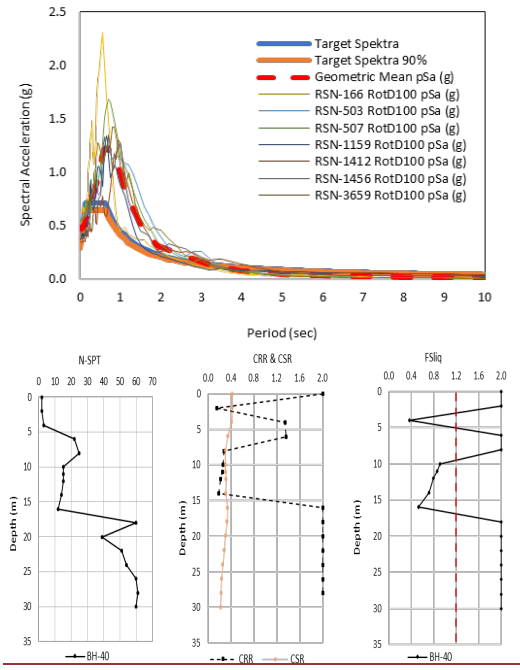

Abstract

The design of building structures requires compliance with seismic codes and all their consequences. Based on geotechnical investigation reports, the construction of Sei Wampu Bridge in Langkat, North Sumatra, Indonesia, is located in an area where the soil layers are predominantly sand with shallow water levels because of its proximity to a river and is a high earthquake zone due to the Semangko fault. That condition will affect the potential of liquefaction occurring. This study aims to identify the liquefaction potential in the Sei Wampu Bridge. Based on *Indonesian National Standard* (SNI) 1726-2019, sites prone to liquefaction are categorized as site class-specific soil (F) and requires site-specific response analysis (SSRA) methods. Non-linear analysis 1-D is chosen to propagate earthquake waves with the software DEEPSOIL V7. The input parameter for soil movement utilizes an average spectral matching method with a minimum of 7 pairs of soil movement selected from the earthquake recording website, PEER Ground Motion Database. The selection of earthquake considers a 1000-year earthquake load return period, or a 7% probability exceeded within 75 years. Site-specific response analysis (SSRA) resulted in a peak ground acceleration (*PGA*) value for each borehole depth used in liquefaction potential analysis. Using a historical earthquake scenario with a 6.3 M_w shows that the research location has liquefaction potential at 0 m-15 m deep with high vulnerability levels, where the LPI value reaches 36.21.

Keywords: Site response analysis, peak ground acceleration, liquefaction, liquefaction potential index, simplified procedure.

1.0 INTRODUCTION

The Indonesian government constructed the Trans Sumatra toll road to accelerate national economic growth and boost regional development in Sumatra according to the Indonesian Economic Acceleration and Expansion Masterplan (MP3I) 2010–2025 [1]. One of the segments prioritized in construction is the 58-kilometer-long Binjai–Langsa Toll segment. At STA 23+175–23+425 crossing the Sei Wampu River, the bridge will be constructed to connect the Stabat subdistrict to the Stabat Lama subdistrict in Langkat Regency, North Sumatra.

The building of infrastructure must consider preventing damage due to natural disasters. Earthquakes are natural disasters that occur frequently on toll roads [2]. Earthquakes can cause major damage to it surrounding areas. Liquefaction is a

disaster that can be triggered by an earthquake [3, 4, 5]. Soil liquefaction is a phenomenon where the soil in a saturated state loses most of its strength and stiffness as a response when given pressure, usually due to earthquakes or sudden changes in pressure, which causes it to behave like a liquid.

The failure of soil from liquefaction is the main cause of bridge damage due to earthquakes. Bridges spanning rivers are very vulnerable to liquefaction as such structures are usually erected on alluvium floodplains, areas with shallow groundwater levels [6].

The extent of infrastructure damage depends on the magnitude, depth, duration of the earthquake, geologic conditions, geotectonic, and ground acceleration at a location from an earthquake. One of the methods to anticipate the direct effects of an earthquake is to design bridge structures resilient to shock.

Bridge structure design needs to consider earthquake aspects and the effect of its location to determine a response spectrum design suitable to the class site. Seismic loads for bridge structures in Indonesia are regulated by the Indonesian National Standard (SNI) 2833:2006 [7] and Earthquake Source and Hazard Map 2017 [8]. The profile characteristics of soil layers with the potential of collapse due to seismic loading, such as soil vulnerable to liquefaction [9]. Site criteria of such soil are categorized as specific soil (SF). There are specific provisions when determining response spectra: propagating earthquake waves from the bedrock using site-specific response analysis (SSRA) methods.

Several researchers have researched the effect of liquefaction on a non-linear response [10, 11]. The research location close to a river observed location effects due to soft soil layers and liquefaction, which effectively changed the amplitude and the frequency of soil movement. A series of parametric analyses to evaluate non-linear seismic soil response had been applied in New Madrid [12]. This region has experienced an 8–8.3 M_w earthquake on top of the area having liquid-behaving soil. The results show that more energy is absorbed during the process, resulting in lower spectral acceleration than the soil surface due to increased damping. Spectral acceleration is critical to know the influence of structural seismic design [13].

Therefore, this research attempts to conduct a 1-D site-specific response analysis (SSRA) [14] for the location of Sei Wampu Bridge on the Binjai-Langsa Toll Road Segment using DEEPSOIL V7. A non-linear (NL) analysis approach is selected to illustrate the suitability of soil layers. The result of SSRA is the *PGA* value on the surface. The value of *PGA* provides an essential parameter in the planning and designing of earthquake-resilient bridge structures to decrease seismic hazards. Furthermore, potential liquefaction evaluation is conducted to achieve safety factor value and used in the Liquefaction Potential Index (LPI) calculation to achieve the liquefaction vulnerability level.

2.0 METHODOLOGY

2.1 Study Area

The research location is a bridge construction site downstream of the Sei Wampu River, which is a part of the Binjai-Langsa Toll Road Segment, located on STA 23+175–23+425 at 3.736° N latitude and 98.394° E longitude. The bridge is classified as a steel-frame continuous arch bridge with three spans measuring lengthwise 231,110 m, widthwise 26,9 m, and a peak height of 14 m.

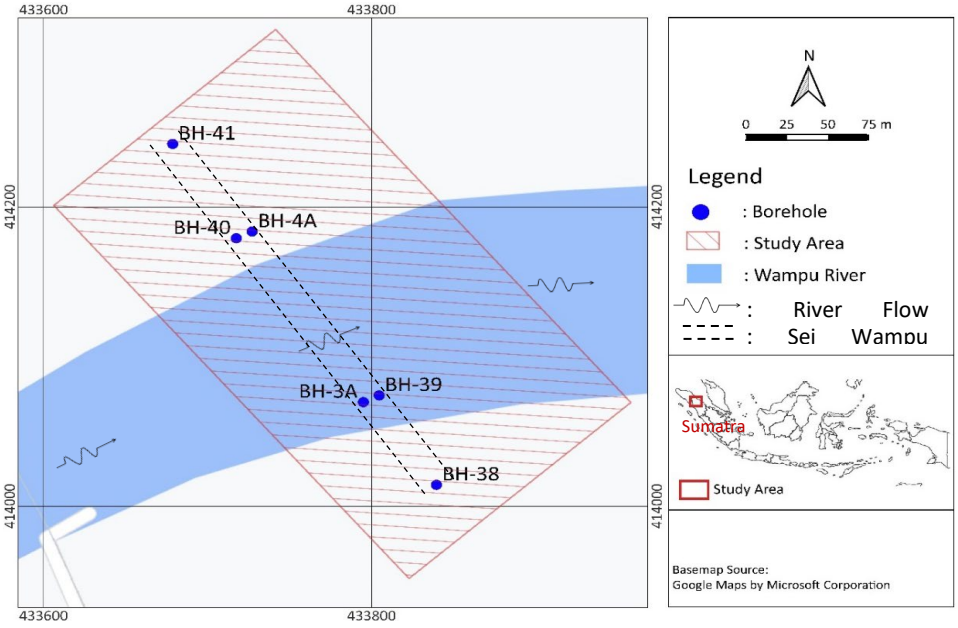

Figure 1 Research Study Area

Figure 1 is the location of the Sei Wampu Bridge, a part of the Binjai–Langsai Toll Road Segment that connects Stabat and Stabat Lama subdistricts. The Sei Wampu Bridge construction project conducts a boring of 4 drills in August 2022 at each placement to ensure the soil layer condition and an additional 2 drills of new boring in January 2023. The initial 4 drills were bored to 30 m, while the 2 new drills were bored to 60 m with two-meter intervals to acquire information on soil layer conditions.

The Sei Wampu Bridge is located in the middle of a railroad and the Sei Wampu Dam. This bridge is close to the downstream of the river. The Sei Wampu Dam is not yet operational despite being built. The construction process of the Sei Wampu Bridge will be disrupted if the Sei Wampu Dam is active. Because the bridge's location is close to the downstream of the river, it is estimated that the river water level will increase along with the operation of the Sei Wampu Dam later.

Figures 2 and 3 are Bridge Embankment Boundaries and the location of Sei Wampu Bridge. The fluctuations of flood water level will be considered in this research due to the location and the position of the bridge pier in the river.

Based on observations on November 11, 2021, the river water level rose by ± 2 m above the benchmark, from an elevation of 8.87 to 10.60 m. It indicates that the river flood water level has approached the bridge abutments. In addition, the planned maximum river discharge, as shown in Figure 4, will reach an elevation of 15.10 m, which means that all the pillars of the Sei Wampu bridge will sink. Therefore, based on the data above, the analysis will use the worst-case scenario, where all the pillars and abutments of the Sei Wampu Bridge will sink, and the soil at the research location will be completely saturated or submerged.

The groundwater level is important to estimate the trigger of liquefaction, as liquefaction does not occur above unsaturated soil. The existing groundwater levels taken during soil investigation are at varying elevations, as shown in Figure 7 interpretation of the soil profile cross-section.

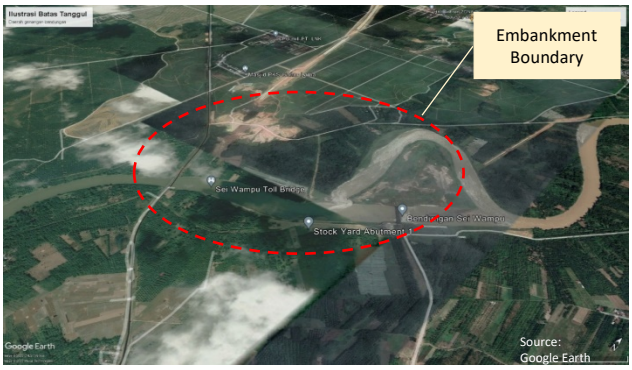

Figure 2 Bridge Embankment Boundaries Interpretation

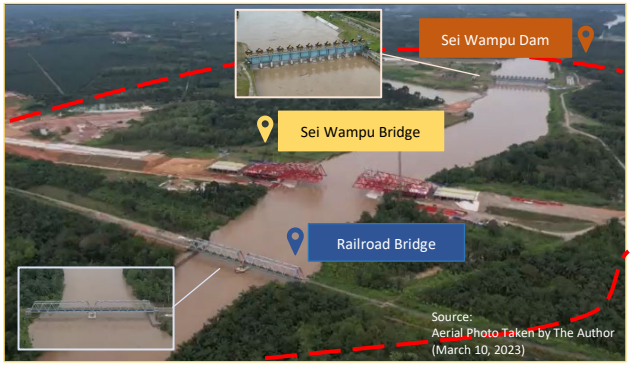

Figure 3 Location of Sei Wampu Bridge

The Sei Wampu Bridge has an effective bridge period of 2.49 s, taken from the Sei Wampu Bridge upper structure report conducted by PT Virama Karya, the design consultant. The bridge is designed using Seismic Isolator-Pendulum bearing to muffle vibrations or earthquakes.

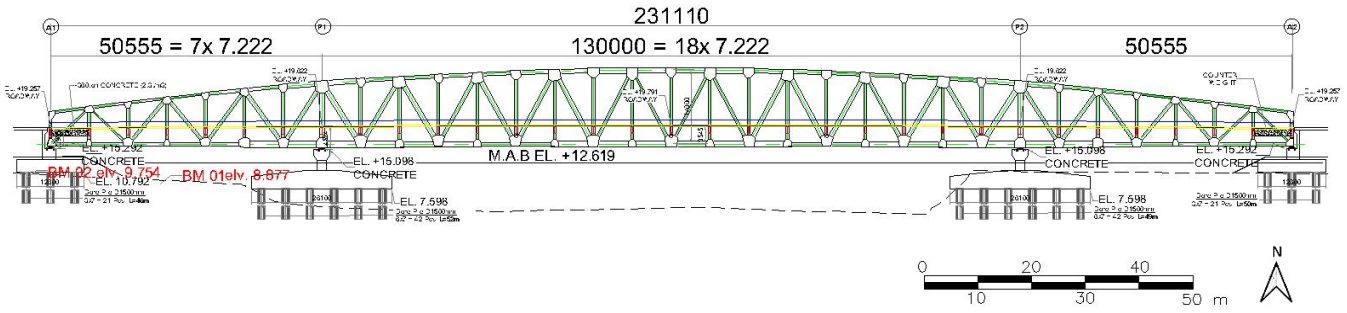

Figure 4 Bridge Water Surface Elevation
(Obtained from PT Hutama Karya report as a contractor of the project)

2.2 Earthquake Source Mechanism

Sumatra is located within a high earthquake zone from the Semangko Fault. The Semangko Fault spans over 1.900 km (from Semangko Bay in South Lampung to Banda Aceh). It spans parallel to a subduction zone as part of the convergence of the Eurasia and Indo-Australia Plates [15].

The Semangko Fault is shaped by the collision force of the Indian Ocean plate to the west that moves below the island of Sumatra to its east. The effect of plates colliding in Sumatra includes the formation of volcanoes, the Semangko Fault, and seismic activity the length of Sumatra [16]. The earthquakes mainly occur in Sumatra and are located in the plate subduction zone and along the Semanko Fault zone. Earthquakes from the plate subduction zone have magnitudes of around 4–8.2 M_w and are situated along the coast, while earthquakes from the Semangko Fault have approximately 4–7.4 M_w. Faults are weak zones, therefore, are susceptible to shifting when shaking

occurs. In Northern Sumatra, many earthquakes occur on land with a magnitude between 6–6.9 M_w ($6 \leq M_w \leq 6.9$) [17].

Based on USGS earthquake data from the past 30 years (1992–2022) within a 500-km radius of the research location [18], earthquake data acquired are those with a magnitude larger than 5 M_w as the minimum boundary that can cause the occurrence of liquefaction with a depth of less than 300 km [19]. Figure 5 shows 3 earthquakes closest to the location, of which is selected an earthquake with a 6.3 M_w located at 61.065 m with a depth of 33 km to be used as the basis for liquefaction calculation for the research.

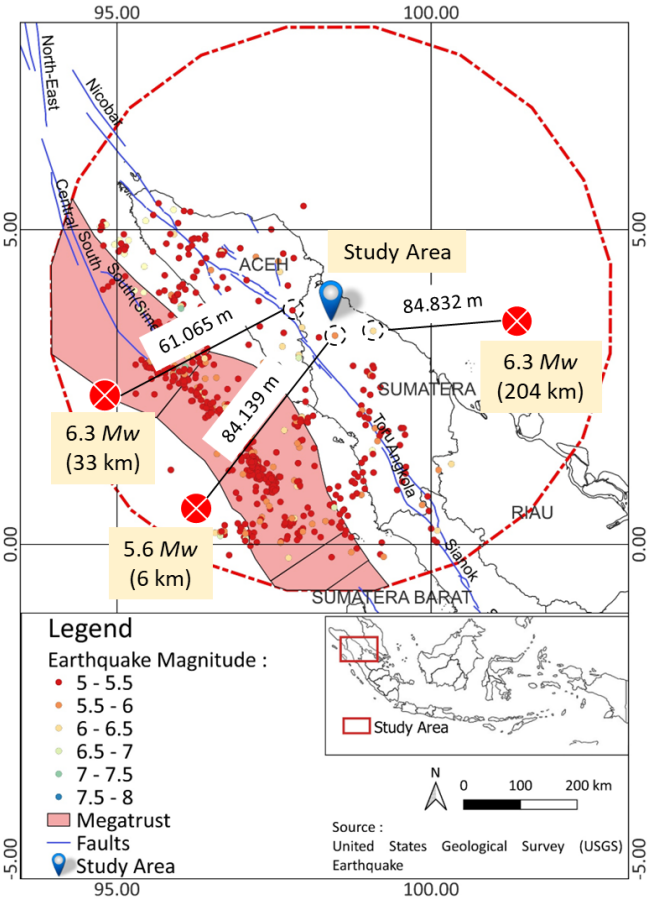

Figure 5 Earthquake Source in the research area

2.3 Geological and Geotechnical Condition

The geological condition of the location of Sei Wampu Bridge (STA 23+175–23+425) is the formation of Alluvium rocks (Qh), including gravel, sand, and clay classified as new deposits or quarter deposits (Holocene). Quarter deposits are generally loose, decomposed, soft, and less compact. Newly deposited soil tends to be more vulnerable to liquefaction than soil deposited over time [20].

Figure 7 shows the interpretation of the soil profile cross-section and the Standard Penetration Test (SPT) of 4 borehole points, 2 initial boring points of the abutment (BH-38 & BH-41), and 2 new boring points of the bridge piers (BH-3A & BH-4A). The boring of 2 initial points was 30 m, while the boring of 2 new points was done to a depth of 60 m with a two-meter interval to obtain information regarding soil layer conditions. The condition of the underground layer for the investigated location showed a dominance of granular material SM (silty sand) and CL (silty clay) for four old bore points in the initial depth of 6 m. Two new boring points showed similar soil properties dominated by granular material SM (silty sand), CH (clay), and GM (silty gravel with sand) at a depth of 17–25 m, resulting in a high *N*-SPT value.

The grain size of soil affects the possible occurrence of liquefaction. Soil with small grains tends to be more vulnerable to liquefaction than large grains. Figure 6 illustrates the plotting of the grain size gradation juxtaposed with Tsuichida's (1970) curve for boreholes BH-38R, BH-39R, BH-40R, and BH 41R. Grain size tests were taken at three points with a depth of 5 m–5.5 m, 10 m–10.5 m, and 15 m–15,5 m for each borehole. In contrast, the grain size test for BH-3A and BH-4A was conducted at a depth range of 1–1.45 to 15–15.45 with depth intervals of 2 meters. Fine content (FC) results have varying values, with the lowest score of 1.5% at BH-3A with a depth of 5 m–5.45 m and the highest FC at 38% at BH-4A with a depth of 13 m–13.45 m.

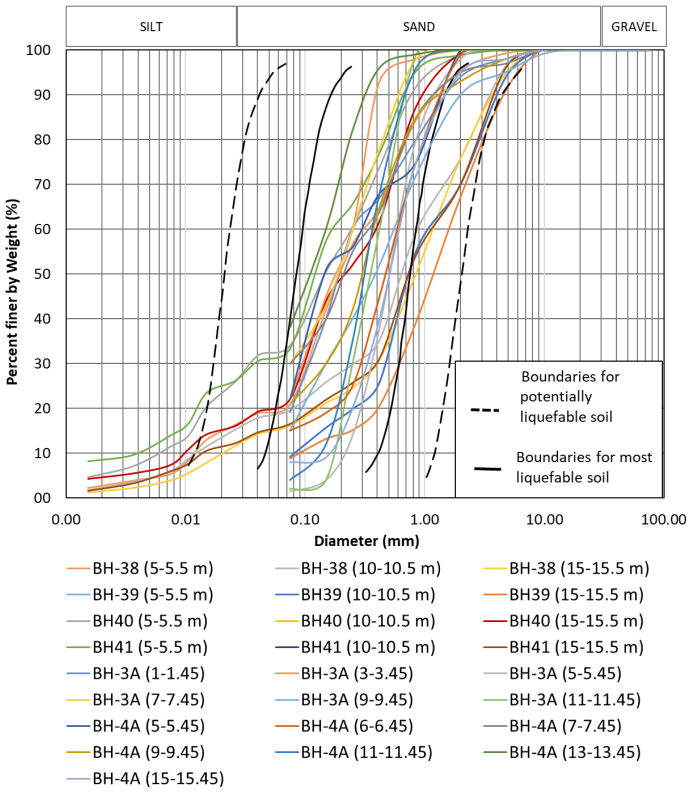

Figure 6 Grain Size Analysis

Location response analysis requires soil investigation data detailed with layer information regarding the *N*-SPT value, shear wave velocity, total unit weight, thickness, and soil type. Meanwhile, there is a lack of data on the in-situ shear wave velocity profile and geophysical test data for the study area. Shear wave speed to determine site class is based on V_{s30} data downloaded from the United States Geological Survey (USGS) database. According to [9], the location is categorized as site class medium soil (D) with V_{s30} between 175 m/s and 350 m/s (350 m/s > V_{s30} > 175 m/s). In this research, the geotechnical investigation is limited to available *N*-SPT data.

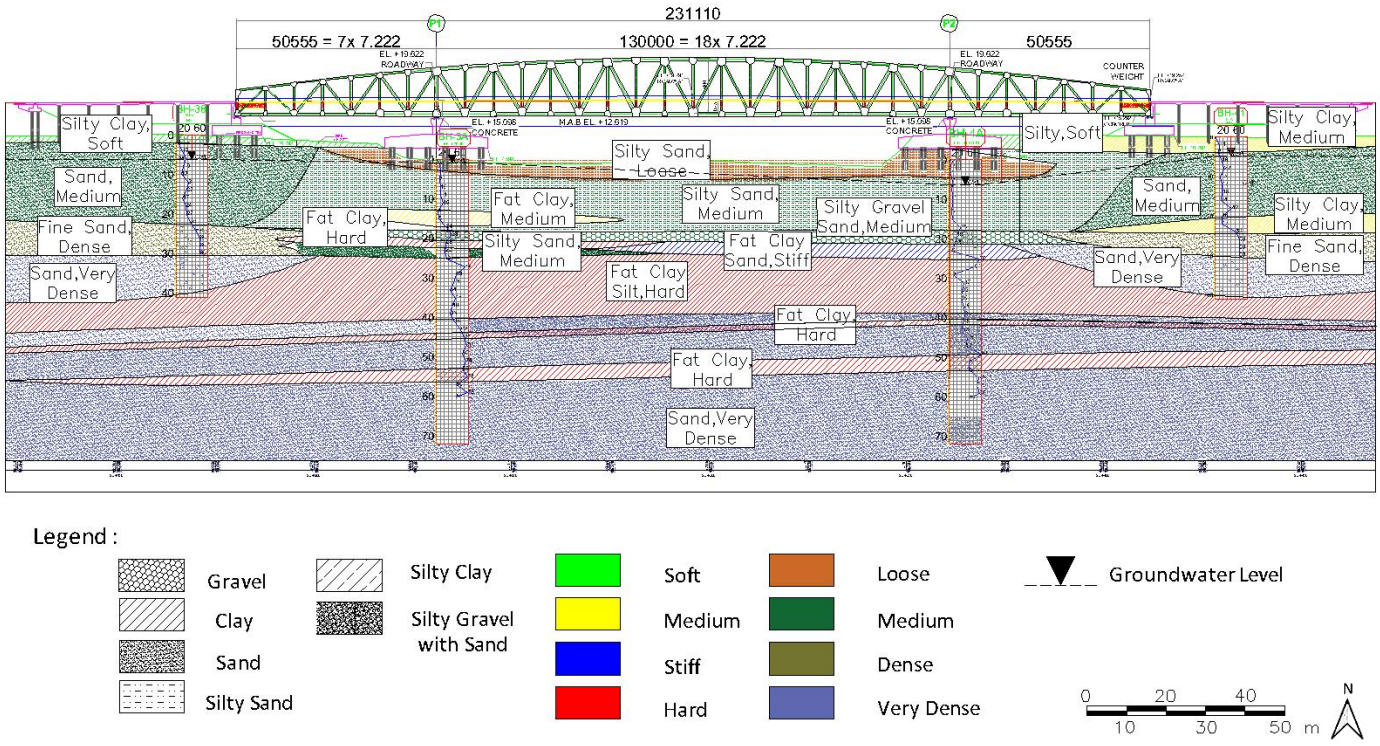

Figure 7 Soil Layer Interpretation

2.4 Non-linear Seismic Response Analysis

2.4.1 Input Motion

Due to the lack of earthquake time history, the spectrum target uses the average spectral matching method with a minimum of 7 soil movements selected [7]. Earthquake observations for other locations are taken from the PEER Ground Motion Database website. Synthetic earthquake characteristic is based on magnitude (M) and distance (R) from the earthquake center, including megathrust, Benioff, shallow fracture, and all source with a 1000-year return period or a 7% probability exceeded within 75 years [21]. M-R value for each source is taken for peak acceleration vibration period (*PGA*), S_a = 0.2 s, dan S_a = 3.0 s. The selection of acceleration recording also considers the influence of significant duration D_{595} using an equation (Kempton & Stewart, 2006) [22]. Significant duration D_{595} is defined as the length of interval time where energy is lost within 5-95% of total earthquake ground motion acceleration energy.

Spectrum response target based on Probabilistic Seismic Hazard Analysis (PSHA) site class medium soil (D) in accordance to code [9]. Spectral response at ground level is determined from three peak acceleration values referring to the Indonesian earthquake map with a probably exceeding 7% within 75 years (*PGA*, S_S, and S_1) and amplification factor values F_{PGA}, F_a, and F_v. After multiplication, the S_a, S_{DS}, and S_{D1} value is obtained at 0.327, 0.714, and 0.453, respectively. The spectrum response target of the research location is presented in Figure 8.

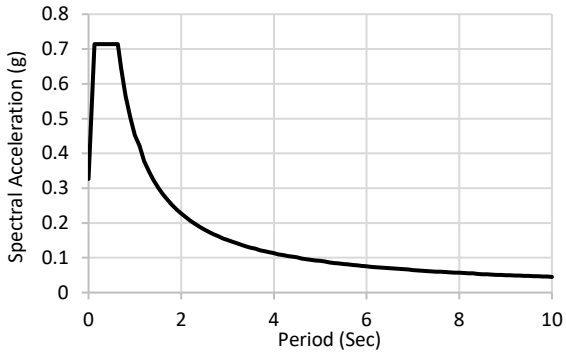

Figure 8 Spectrum Target

Ground movement modification is conducted by using the amplitude scaling method. This method refers to [9] using spectral data RotD100 for each record [23]. It is then scaled and averaged until the spectral acceleration value for the reviewed period exceeds or is equal to 90% of the spectrum target. The result of amplitude scaling is between 2.3–3.7, following the recommendation of Zaereian and Zhong [24], which is that it does not exceed 5 to maintain ground movement characteristics representative of actual earthquake occurrence. The period range for ground movement modification is determined by [7], which is between 0.5T_f minimum fundamental period (T_{min}) and 2T_f fundamental maximum period (T_{max}). This structure's value for T_{min} and T_{max} is 1.25 seconds and 4.98 seconds, respectively.

Table 1 Ground Motion and Scaling Recording

No	Code	Earthquake Name	Year	Station	Mag (M_w)	R_{rup} (km)	D_{5-95} (s)	Scale Factor
1	166	Imperial Valley-06	1979	Coachella Canal #4	6.53	50.1	11.1	3.78
2	503	Taiwan SMART1(40)	1086	SMART1 COO	6.32	59.92	13.3	2.42
3	507	Taiwan SMART1(40)	1986	SMART1 M01	6.32	60.86	9.8	3.08
4	1159	Kocaeli, Turkey	1999	Eregli	7.51	142.29	23.2	3.31
5	1412	Chi-Chi, Taiwan	1999	TAP006	7.62	105.66	21	2.41
6	1456	Chi-Chi, Taiwan	1999	TAP095	7.62	109	15.5	2.39
7	3659	Taiwan SMART1(40)	1986	SMART1010	6.32	59.96	14.8	2.94

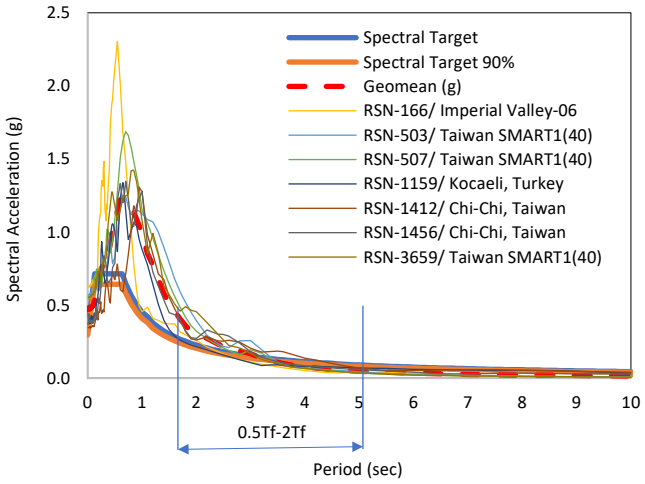

Figure 9 Response Spectrum Scaling

Figure 9 presents the results of synthetic ground motion scaling following the spectrum target specified. The resulting synthetic ground motion is used as DEEPSOIL V7 input. The recapitulation of the ground motion selected, and the scale factor is presented in Table 1. The response spectra curve is plotted in Figure 10. Even though site-specific response analysis (SSRA) is conducted, the proposed response spectrum design must comply with the regulation. It is recommended that the value of spectral design acceleration for each period cannot be less than 80% of the spectral acceleration determined for the type E soil profile [9].

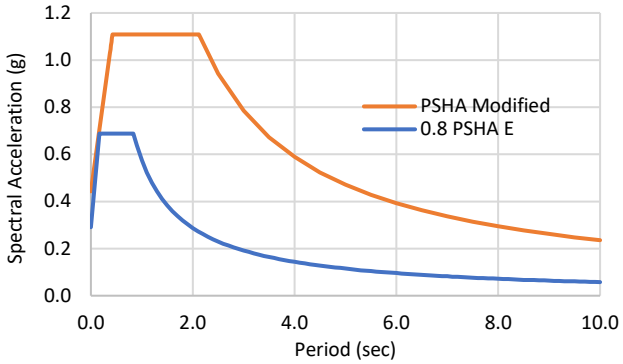

Figure 10 Comparison of Response Spectrum Surface SSRA and Response Spectrum Surface Class E

2.4.2 Site Response Analysis

Site-Specific Response Analysis (SSRA) is the process of propagating seismic waves from the bedrock through the overlying soil layers up to the surface. This analysis can be obtained by directly multiplying the response spectrum at the bedrock with specific amplification factors recommended in [7]. Site Specific Response Analysis (SSRA) considers the geotechnical characteristics of soil and rocks around the site, such as soil type, density, shear strength, and modulus of elasticity [25].

Modeling in this analysis utilizes the DEEPSOIL V7. DEEPSOIL is a software program designed for one-dimensional site response analysis. It offers the capability to: a) 1-D nonlinear time domain analyses with and without pore water pressure generation, b) 1-D equivalent linear frequency domain analyses including convolution and deconvolution, and c) 1-D linear time and frequency domain analyses[14].

This research applies a 1-D nonlinear time domain analysis method (GQ/H Soil Model with Non-Masing Re/Unloading Behavior) [14]. Generalized Quadratic/hyperbolic (GQ/H) is a method that can represent the non-linear characteristic of small strains and soil shear strength [26]. This method is a model of one dimension shear stress-strain simplified to overcome model limitations often found within non-linear site response analysis. The input parameter for the soil profile in DEEPSOIL is presented in Table 2. Equation 1 is used to measure Maximum Shear Strength (τ_{max}).

$$\tau_{max} = c_{vs} + \sigma'_{vc} \times tan(\phi) \quad (1)$$

$$\phi = [15.4(N_1)_{60}]^{0.5} + 20 \quad (2)$$

where ϕ = soil friction angle (degrees), σ'_{vc}= effective stress (kPa) at the center layer of soil, c_{vs} = shear strength (kPa) based on valuation developed from 0,1% shear strain for linear elastic material with 80% maximum shear modulus originating value V_s soil layer observed.

$$G_{max} = \rho V_s^2 \quad (3)$$

$$C_{vs} = \rho V_s^2 \times 0{,}8 \times 0{,}1\% \quad (4)$$

where: G_{max}= shear modulus (Mpa), ρ = weight of soil (kN/m^2), and V_s= shear wave velocity (m/s) from Equation 21 to 23 [27].

$$\ln(V_s) = 4.045 + 0.0961\ln(N_{60}) + 0.236\ln(\sigma'_{v0}) : \text{sand} \quad (5)$$

$$\ln(V_s) = 3.783 + 0.178\ln(N_{60}) + 0.231\ln(\sigma'_{v0}) : \text{silt} \quad (6)$$

$$\ln(V_s) = 3.996 + 0.230\ln(N_{60}) + 0.164\ln(\sigma'_{v0}) : \text{clay} \quad (7)$$

where N_{60} = *N*-SPT value corrected for a 60% efficiency, and σ'_{vc}= effective stress (kPa). Determining the soil thickness requires checking the maximum frequency (f_{max}), generally with a minimum of 30 Hz [14].

The input parameter to select the reduction modulus curve and appropriate damping proposed by [28] is Plasticity Index (PI), soil pressure coefficient at idle conditions (K_0) can be calculated by:

$$K_0 = [1 - sin(\phi)] \times OCR^{sin\,(\phi)} \quad (8)$$

where: ϕ= soil friction angle (degrees), *OCR* = over consolidation ratio, with a value 1 chosen [28].

Table 2 Input Parameter for Soil Profile BH-40

No	Depth (m)	Thickness (m)	γ_b (KN/m³)	γ_{sat} (KN/m³)	Category	N_{60}	$(N_1)_{60}$	σ_{VC} (kPa)	σ'_{VC} (kPa)	V_s (m/s)	ϕ	c_{vs} (kPa)	τ_{max} (kPa)	K_0	PI
1	0.5	0.5	16.06	18.00	Clay	2.05	3.48	8.03	4.09	80.80	27.32	9.58	10.46	0.54	10.56
2	1	0.5	16.06	18.00	Clay	2.05	3.48	16.06	8.19	90.52	27.32	12.03	12.91	0.54	10.56
3	1.5	0.5	16.06	18.00	Clay	2.05	3.48	24.09	12.28	96.75	27.32	13.74	14.62	0.54	10.56
4	2	0.5	16.06	18.00	Clay	2.05	3.48	32.12	16.37	101.42	27.32	15.10	15.98	0.54	10.56
5	2.5	0.5	16.06	18.00	Clay	2.05	3.48	40.15	20.46	105.20	27.32	16.25	17.13	0.54	10.56
6	3	0.5	16.06	18.00	Clay	2.05	3.48	48.18	24.56	108.40	27.32	17.25	18.13	0.54	10.56
7	3.5	0.5	16.06	18.00	Clay	2.05	3.48	56.21	28.65	111.17	27.32	18.14	19.02	0.54	10.56
8	4	0.5	16.19	18.14	Sand	3.07	5.22	64.30	32.81	144.97	28.97	31.10	32.04	0.52	10.56
9	4.5	0.5	16.19	18.14	Sand	3.07	5.22	72.40	36.98	149.12	28.97	32.90	33.84	0.52	10.56
10	5	0.5	16.19	18.14	Sand	3.07	4.99	80.49	41.14	152.92	28.76	34.60	35.49	0.52	10.56
11	5.5	0.5	16.19	18.14	Sand	3.07	4.74	88.59	45.30	156.44	28.55	36.21	37.05	0.52	10.56
12	6	0.5	18.65	20.82	Sand	22.52	28.43	97.91	50.81	194.61	40.92	64.33	65.42	0.34	10.56
13	6.5	0.5	18.65	20.82	Sand	22.52	27.55	107.24	56.31	199.40	40.60	67.53	68.58	0.35	10.56
14	7	0.5	18.65	20.82	Sand	22.52	26.75	116.56	61.82	203.83	40.30	70.57	71.58	0.35	10.56
15	8	1	19.04	21.24	Sand	25.59	28.53	135.60	73.25	214.78	40.96	79.95	80.92	0.34	10.56
16	9	1	19.04	21.24	Sand	25.59	27.35	154.63	84.69	222.26	40.52	85.61	86.53	0.35	10.56
17	10	1	15.06	17.04	Sand	15.36	16.05	169.69	91.92	215.76	35.72	64.73	65.48	0.42	8.41
18	11	1	15.06	17.04	Sand	15.36	15.49	184.75	99.16	219.65	35.45	67.08	67.80	0.42	8.41
19	12	1	15.06	17.04	Sand	15.36	14.98	199.81	106.39	223.33	35.19	69.35	70.04	0.42	8.41
20	13	1	15.06	17.04	Sand	15.36	14.51	214.87	113.63	226.83	34.95	71.54	72.20	0.43	8.41
21	14	1	14.93	16.92	Sand	14.33	13.12	229.80	120.73	228.58	34.21	72.10	72.73	0.44	8.41
22	15	1	14.93	16.92	Sand	14.33	12.73	244.73	127.84	231.69	34.00	74.08	74.68	0.44	9.98
23	16	1	14.67	16.66	Sand	12.29	10.56	259.39	134.69	231.11	32.75	72.60	73.15	0.46	9.98
24	17	1	14.67	16.66	Sand	17.40	14.79	274.06	141.54	241.79	35.09	79.46	80.06	0.43	9.98
25	18	1	20.98	22.79	Sand	28.67	24.17	295.03	154.52	258.96	39.29	124.68	125.37	0.37	9.98
26	19	1	20.98	22.79	Sand	28.67	23.32	316.01	167.50	263.93	38.95	129.52	130.17	0.37	9.98
27	20	1	18.22	20.11	Sand	53.24	45.87	334.22	177.80	284.07	46.58	132.38	133.29	0.27	9.98
28	21	1	18.22	20.11	Sand	53.24	45.17	352.44	188.10	287.87	46.37	135.94	136.83	0.28	9.98
29	22	1	19.79	21.64	Sand	53.24	44.29	372.23	199.93	292.04	46.12	150.57	151.44	0.28	9.98
30	23	1	19.79	21.64	Sand	53.24	43.46	392.03	211.77	296.03	45.87	154.72	155.56	0.28	9.98
31	24	1	20.19	22.02	Sand	61.43	49.81	412.22	223.98	304.12	47.70	166.18	167.07	0.26	9.98
32	25	1	20.19	22.02	Sand	61.43	49.12	432.40	236.20	307.96	47.50	170.40	171.27	0.26	9.98
33	26	1	20.98	22.79	Sand	61.43	48.43	453.38	249.18	311.87	47.31	180.84	181.69	0.26	9.98
34	27	1	20.98	22.79	Sand	61.43	47.79	474.36	262.16	315.63	47.13	185.22	186.06	0.27	9.98
35	28	1	21.11	22.92	Sand	61.43	47.18	495.47	275.27	319.29	46.96	190.60	191.42	0.27	9.98
36	29	1	21.11	22.92	Sand	61.43	46.61	516.57	288.37	322.81	46.79	194.83	195.64	0.27	9.98
37	30	1	20.98	22.79	Sand	61.43	46.07	537.55	301.36	326.19	46.64	197.82	198.61	0.27	9.98

2.5 Liquefaction Potential Analysis

2.5.1 Simplified Procedure

The procedure required to evaluate liquefaction potential is conducted in two steps, evaluating seismic loading and soil strength towards seismic loading. The safety factor is calculated from the cyclic stress ratio (CSR) and Cyclic Resistance Ratio ($CRR_{7.5}$), as shown in Equation 9. Liquefaction is estimated to occur when FSliq < 1.2 [29]

$$FS_{Liq} = \frac{CRR_{M=7.5,\sigma'_{vc}=1}}{CSR_{M=7.5,\sigma'_{vc}=1}} < 1.2 \quad (9)$$

Cyclic Resistance Ratio is the ratio between peak cyclic resistance and effective vertical stress. Idriss & Boulanger (2008) [30] determines the correlation between CRR and N-SPT values, illustrated in equations 10-11.

$$CRR_{M=7.5,\sigma'_{vc}=1} = exp\left(\frac{(N_1)_{60cs}}{14.1} + \left(\frac{(N_1)_{60cs}}{126}\right)^2 - \left(\frac{(N_1)_{60cs}}{23.6}\right)^3 + \left(\frac{(N_1)_{60cs}}{25.4}\right)^4 - 2.8\right) \quad (10)$$

$$CRR_{M;\sigma'_{vc}} = CRR_{M=7.5,\sigma'_{vc}=1} \times MSF \times K_\sigma \quad (11)$$

where $(N_1)_{60cs}$ is the correction factor of fines content, $CRR_{M;\sigma'vc}$ is the CRR value for the other moment magnitude earthquake, K_σ is a factor correction of overburden, and MSF is Factor Scaling of earthquake magnitude. The value of MSF is calculated according to Idriss & Boulanger (2014) [31] and is shown in equations 12-13.

$$MSF = 1 + (MSF_{max}) \left(8.64\, exp\left(\frac{-M}{4}\right) - 1.325\right) \quad (12)$$

$$MSF_{max} = 1.09 + \left(\frac{(N_1)_{60cs}}{31.5}\right) \leq 2.2 \quad (13)$$

where MSF_{max} is the new MSF developed by Idris & Boulanger for soil conditions. Cyclic Stress Ratio (CSR) is the shear strain from an earthquake. CSR occurs when soil receives a seismic load. The most important factor in determining CSR is determining peak ground acceleration. CSR calculation is shown in Equation 14 and is analyzed using the method developed by Idriss & Boulanger (2008) [30] based on *N*-SPT values.

$$CSR_{M=7.5,\sigma'_{vc}=1} = 0.65 \left(\frac{a_{max}}{g}\right)\left(\frac{\sigma_{vc}}{\sigma'_{vc}}\right) r_d \quad (14)$$

where σ_{vc} is the total vertical stress, σ'_{vc} is the effective vertical stress r_d is the stress reduction coefficient, and a_{max} is the maximum peak ground acceleration.

2.5.2 Liquefaction Potential Index (LPI)

Liquefaction Potential Index (LPI) is a method first introduced by Iwasaki et al. (1984) [32] and used to estimate the potential of liquefaction based on liquefaction severity and liquefaction zone depth. LPI value is calculated based on the liquefied soil layer's thickness, depth, and safety factor. This method is calculated up to 20 m below ground level.

Severity level categories due to liquefaction by Iwasaki et al. (1984) does not yet define the degree of vulnerability for the category of not liquefied and moderate. To overcome this limitation, Sonmez (2003) [33] modifies the LPI of Iwasaki et al. (1984) by adding boundaries and categories. The value of LPI is calculated using the following equation:

$$LPI = \int_0^{20} F.w(z)dz \quad (15)$$

With:

$$F = 0\ for\ SF\ \geq 1.2 \quad (16)$$

$$F = 1 - SF\ for\ SF\ < 0.95 \quad (17)$$

$$F = 2 \times 10^6 e^{-18.427(SF)} for\ 0.95 < SF < 1.2 \quad (18)$$

$$w(z) = 0\ for\ z\ > 20\ m \quad (19)$$

$$w(z) = 10 - 0.5z\ for\ z\ < 20\ m \quad (20)$$

where F is the damage level of a layer in liquefaction analysis and $w(z)$ is the depth weight factor, where z is the depth under consideration, maximum up to 20 m. The value of LPI was classified into several categories, as shown in Table 3.

Table 3 Liquefaction Potential Index Classification [33]

LPI Value	Categories
0	Non-liquefied
0 < LPI ≤ 2	Low
2 < LPI ≤ 5	Moderate
5 < LPI ≤ 15	High
LPI > 15	Very High

3.0 RESULTS AND DISCUSSION

3.1 Peak Ground Acceleration

Cyclic Stress Ratio is calculated to determine the seismic load of the soil layer that causes liquefaction. As mentioned, cyclic strain is calculated using DEEPSOIL V7 to obtain peak ground acceleration (*PGA*) for each soil profile. A non-linear analysis determines the influence of the location's soil condition with cyclic strain. In linear analysis, the value of *PGA* will be the same for each depth and is determined by site classification. Meanwhile, the results show that maximum surface acceleration differs for each borehole in the same site classification. Figure 11 shows the *PGA* for each soil layer which is then used to determine the Cyclic Stress Ratio (CSR) value in analyzing liquefaction potential for each depth.

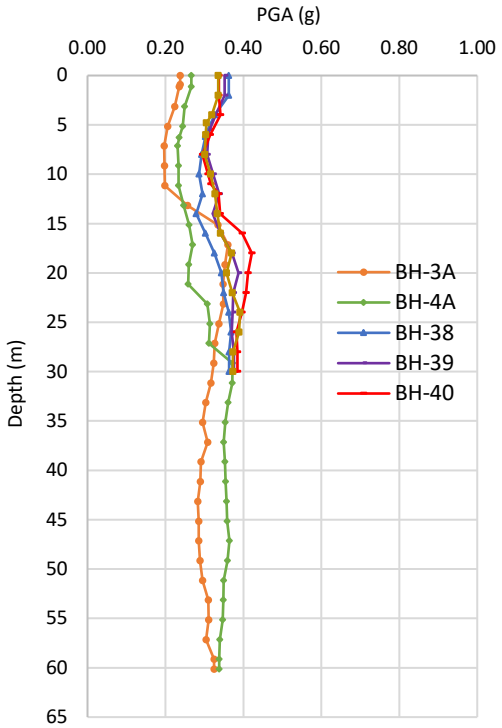

Figure 11 Peak Ground Acceleration (*PGA*) Values

BH-3A and BH-4A resulted in values less than the other four boreholes. The upper soil layer profile is dominated by loose soil that tends to decrease vibration. BH-3A at a depth of 15 m experiences amplification due to a layer of clay that BH-40 also experiences at a depth of 18 m.

Table 4 compares the maximum surface and normal acceleration used in linear analysis. Amplification occurs at four boreholes. BH-38 has the highest value of 0.11. BH-39, BH-40, and BH-41, within a minimal value, between 0.08–0.02, can be considered a condition where amplification does not occur.

Table 4 Summary of Maximum Surface Acceleration and *PGA* according to National Standard of Indonesia (SNI) 2833:2016

Borehole	Surface Maximum Accelerations (g)	*PGA* SNI 2833:2016 (g)	Ratio
BH-3A	0.238	0.327	0.73
BH-4A	0.267	0.327	0.82
BH-38	0.363	0.327	1.11
BH-39	0.352	0.327	1.08
BH-40	0.337	0.327	1.03
BH-41	0.335	0.327	1.02

Peak ground acceleration (*PGA*) is considered necessary in influencing liquefaction. The resulting *PGA* for the location ranges between 0.2g–0.4g, which is supposed to have a risk of high damage [34].

3.2 Liquefaction Potential Evaluation

Before calculating the liquefaction potential numerically, preliminary calculations were carried out on the soil investigation results, namely the grain size distribution. Analysis of grain size distribution was carried out at six boreholes at a certain depth, shown in Figure 8. The average FC value was obtained in the 1.5%–38%. Several studies have shown that soils that are prone to liquefaction are soils with SPT values < 20 and fine grain content ranging from 5–42% [35], and FC > 35% are predicted not to be liquefied [36]. Furthermore, the soil grain size distribution revealed that more than 65% of the soil samples' grains were fine sand [37].

Liquefaction potential analysis is conducted for each borehole with a 6.3 Mw and a distance of 61.10 km earthquake scenario, which is determined as the most significant earthquake between 1992–2022 within a radius of 500 km. The potential liquefaction calculation used each depth's *PGA* value from site response analysis. All borehole points use submergence scenarios in the analysis. It was chosen to plan a conservative structural design. The potential for liquefaction under submergence has a high value [38]. The liquefaction potential safety factor decreases as the groundwater level becomes shallower. The calculation results of the liquefaction potential analysis are shown in Table 6.

An example of the results of the liquefaction potential analysis at BH-40 can be seen in Figure 12. At depths from 0-2 m with soil type classified as clay, FS_{Liq}= 2. Meanwhile, at depths from 3-6 m with soil type classified as sand, FS_{Liq}< 1.2, which has the liquefaction potential when referring to [29]. This is also due to the low *N*-SPT value of 3, causing a low CRR value. With the same soil type for depths of 6 m–10 m, there is no potential for liquefaction due to a high N-SPT value approaching 30, resulting in a high CRR. Liquefaction also occurs at depths of 10 m - 18 m. After a depth of 18 m, the value of FS_{Liq}= 2, resulting in a relatively high *N*-SPT value at that depth (>50). Sand with *N*-SPT values of less than 20 is prone to liquefaction, while sand with *N*-SPT values over 30 is not liquefaction potential. If liquefaction occurs, the soil damage is insignificant [39, 40].

Based on the liquefaction potential analysis conducted for all boreholes, liquefaction occurs at varying depths. This is due to the different soil characteristics for each borehole, as shown in Figure 7. Because BH-3A and BH-4A have loose sand to medium dense from the ground surface to a depth of 20 m, liquefaction occurs at that depth. In contrast, the other four boreholes at the same depth consist of clay and thus do not have the liquefaction potential. The summary of FS_{Liq} values for BH-3A, BH-4A, BH-38, BH-39, dan BH-41, shown in Figures 13-14.

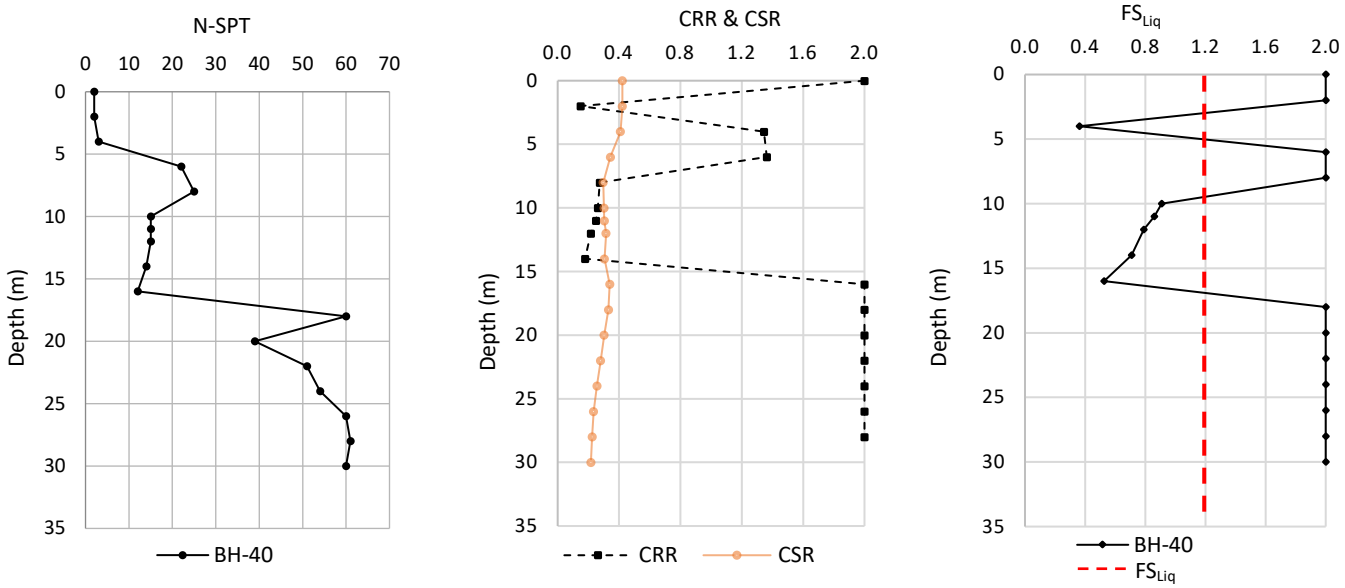

Figure 12 Liquefaction Potential Analysis for BH-40

The FS_{Liq} values for each depth are then used to determine LPI. LPI value shows the soil vulnerability degree towards liquefaction calculated using equation 10. The resulting LPI is classified by categorizing based on vulnerability degree, referred to in Table 3. Recapitulation of LPI calculation results and the categories for all six boreholes are shown in Table 5

Liquefaction Potential Index is calculated using a 6.3 M_w earthquake to a depth of 20 m. The results show a liquefaction vulnerability degree of moderate for BH-38 at 2.09. Meanwhile, a very high degree of liquefaction vulnerability is obtained for BH-4A at 36.21.

Table 5 Liquefaction Potential Index Classification

NO	Bore Hole	LPI	Liquefaction Vulnerability Degree
1	BH-3A	6.49	High
2	BH-4A	36.21	Very High
3	BH-38	2.09	Moderate
4	BH-39	5.90	High
5	BH-40	16.23	Very High
6	BH-41	12.63	High

Table 6 Soil Profile Properties

Depth (m)	*N*-SPT (m)	Soil Type	σ'_{vc} (kN/m²)	*FC* %	α	β	rd	*PGA*	CSR	$(N_1)_{60cs}$	$(N_1)_{60}$	MSF	CRR	$SF_{Liq} < 1.2$	Result
2	2	Clay	16.37	34.12	-0.08	0.01	0.98	0.34	0.42	8.97	3.48	1.08	n.a.	n.a	NL
4	3	Sand	33.02	34.12	-0.20	0.02	0.95	0.34	0.41	10.71	5.22	1.10	0.15	0.36	L
6	22	Sand	55.05	34.12	-0.34	0.04	0.91	0.32	0.34	33.20	27.71	1.56	1.34	2.00	NL
8	25	Sand	77.91	34.12	-0.50	0.06	0.86	0.29	0.30	33.44	27.95	1.56	1.36	2.00	NL
10	15	Sand	92.38	23.67	-0.68	0.08	0.82	0.31	0.30	20.91	15.96	1.25	0.27	0.91	L
11	15	Sand	99.62	23.67	-0.77	0.09	0.79	0.32	0.30	20.40	15.45	1.24	0.26	0.86	L
12	15	Sand	106.85	23.67	-0.87	0.10	0.77	0.34	0.32	19.93	14.98	1.23	0.25	0.79	L
14	14	Sand	121.07	23.67	-1.06	0.12	0.73	0.34	0.31	18.15	13.19	1.20	0.22	0.71	L
16	12	Sand	134.77	22.19	-1.25	0.14	0.68	0.40	0.34	15.48	10.69	1.15	0.18	0.53	L
18	60	Sand	160.73	22.19	-1.43	0.16	0.64	0.42	0.33	59.15	54.36	2.02	2.00	2.00	NL
20	39	Sand	181.33	22.19	-1.61	0.18	0.61	0.41	0.30	38.09	33.30	1.72	2.00	2.00	NL
22	51	Sand	204.99	22.19	-1.76	0.19	0.58	0.41	0.28	48.13	43.34	2.02	2.00	2.00	NL
24	54	Sand	229.42	22.19	-1.89	0.20	0.55	0.40	0.26	49.34	44.55	2.02	2.00	2.00	NL
26	60	Sand	255.38	22.19	-2.00	0.21	0.52	0.38	0.23	52.91	48.12	2.02	2.00	2.00	NL
28	61	Sand	281.60	22.19	-2.08	0.22	0.50	0.38	0.22	52.47	47.68	2.02	2.00	2.00	NL
30	60	Sand	307.56	22.19	-2.12	0.22	0.49	0.38	0.22	50.62	45.82	2.02	2.00	2.00	NL

*)Note: NL = Not Liquefied, L = Liquefied, n.a.= Not Available

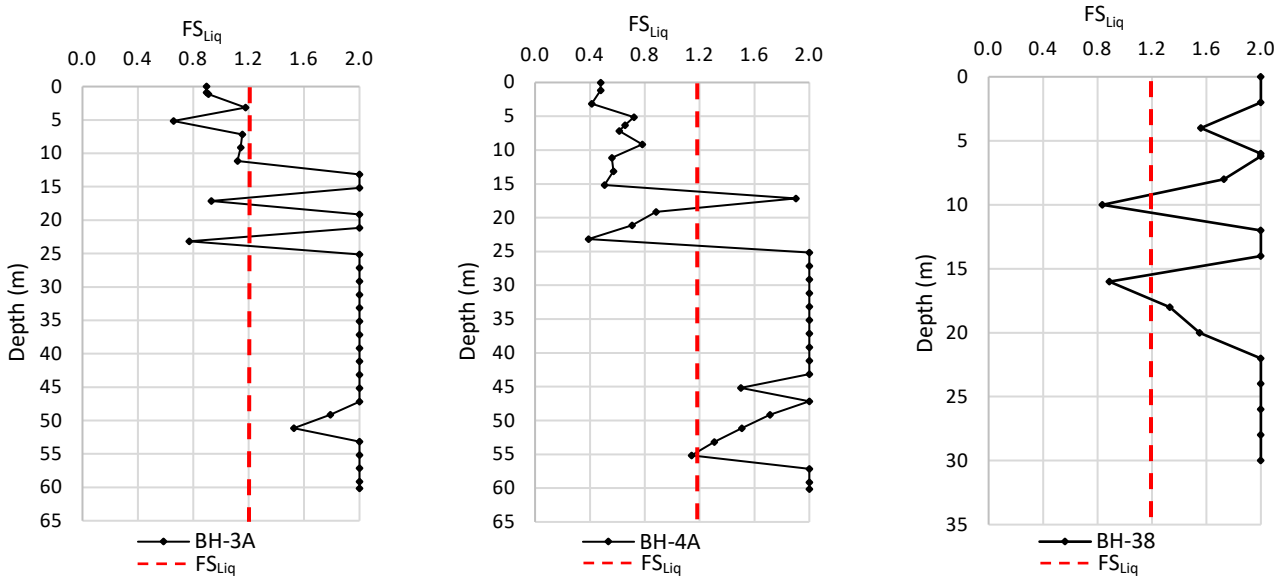

Figure 13 The results of the liquefaction safety factor

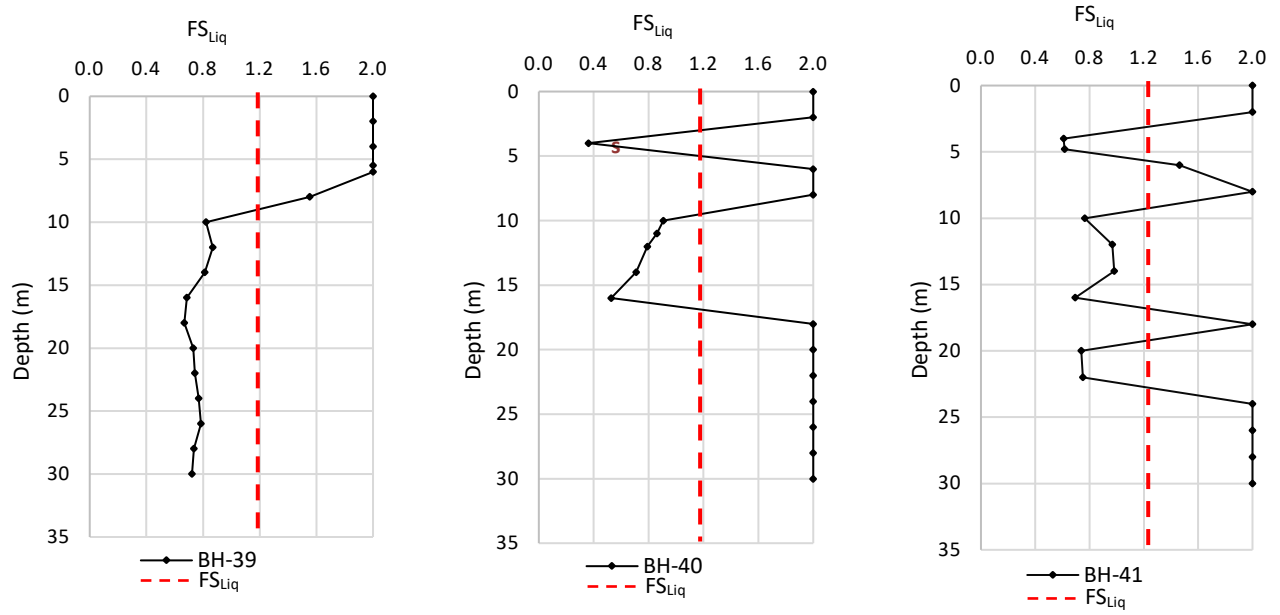

Figure 14 The results of the liquefaction safety factor (continued)

4.0 CONCLUSION

Soil condition is crucial in strengthening ground movement when spreading through soil layers. Studying the dynamic behavior of local soil conditions to determine the seismic hazard of Sei Wampu's locations to design seismic resilient structures with good performance during the entire life cycle is crucial. One thing that needs to be considered is the resistance of the structure to liquefaction phenomena. Based on the analysis that has been carried out, it is found that the location is vulnerable to liquefaction. It is supported by the FC value of less than 35% and dominated by fine sand of more than 65%. The soil layers at the site of Sei Wampu Bridge are classified as medium soil (SD) based on the United States Geological Survey (USGS). Site-specific response analysis (SSRA) has resulted in *PGA* values for each borehole. *PGA* values range between 0.2g – 0.4g. These values constitute a serious damage risk. The seismic parameter uses a historic earthquake scenario of 6.3 M_w. With the worse scenario that all soil layers will be saturated by flood, the liquefaction potential is discovered at a depth of 0 m–20 m, with varying results corresponding to the soil type characteristics for each borehole. LPI value with a vulnerability degree for liquefaction is very high, reaching 36.21. High liquefaction potential in this area needs a mitigation strategy to guarantee the sustainability of bridge infrastructure. However, further studies are needed regarding alternative mitigation options for liquefaction.

Acknowledgement

The authors would like to express their gratitude for the support given by PT Hutama Karya and PT Hutama Karya Infrastruktur Binjai – Langsa, for their assistance with the data of this article.

References

[1] Presidential Regulation Number 100 the Year 2014. 2014. Concerning the Acceleration of Toll Road Development in Sumatra. RI Cabinet Secretariat. Jakarta, Indonesia.

[2] Askaviolita, I., S. Sito, and T.F. Fathani. 2022. Liquefaction Potential Index Analysis In Solo – Yogyakarta – Nyia Kulon Progo Toll Road (Section Karanganyar To Klaten Regency) At Central Java. In *Proceedings of the 5th International Conference On Earthquake Engineering And Disaster Mitigation 2022*.

[3] Pramaditya, A., and T.F. Fathani. 2021. Physical Modelling of Earthquake-induced Liquefaction on Uniform Soil Deposit and Earth Structures Settlement. *Journal of the Civil Engineering Forum.* 85–96.

[4] Das Braja, M., and G.V. Ramana. 2011. *Principles of Soil Dynamics 2nd*. Stamford: Cengage Learning.

[5] Mase, L.Z., T.F. Fathani, and A.D. Adi. 2021. A Simple Shaking Table Test to Measure Liquefaction Potential of Prambanan Area, Yogyakarta, Indonesia. *ASEAN Engineering Journal* 11: 89–108. https://doi.org/10.11113/aej.v11.16874.

[6] Youd, T.L. *Liquefaction-Induced Damage to Bridges*. Vol. 84602. Provo, Utah: Department of Civil Engineering, Brigham Young University.

[7] Indonesian Standard Code. 2016. *Procedures for planning bridges against earthquake loads (SNI 2833:2016*. National Standardization Agency).

[8] National Center for Earthquake Studies: Indonesian Seismic Sources and Seismic Hazard Maps, Center for Research and Development of Housing and Resettlement. 2017. Ministry of Public Works and Human Settlements.

[9] Indonesian Standard Code. 2019. *Earthquake Resistance Design for Buildings*. (*SNI 1726:2019*. National Standardization Agency).

[10] Sil, A., and J. Haloi. 2018. Site-Specific Ground Response Analysis of a Proposed Bridge Site over Barak River along Silchar Bypass Road, India. *Innovative Infrastructure Solutions* 3: 63. https://doi.org/10.1007/s41062-018-0167-y.

[11] Taghavinezhad, M., A.J. Choobbasti, and F. Farrokhzad. 2021. Effect of Liquefaction on Non-linear Seismic Response in Layered Soils: A Case Study of Babol, North of Iran. *European Journal of Environmental and Civil Engineering* 25: 2199–2216. https://doi.org/10.1080/19648189.2019.1623081.

[12] Zheng, W., and L. Ronaldo. 2011. Non-linear Site Response and Liquefaction Analysis in the New Madrid Seismic Zone. *Geotechnical*

and Geological Engineering 29: 463–75. https://doi.org/10.1007/s10706-011-9396-y.

[13] Youd, T.L., and B.L. Carter. Influence of Soil Softening and Liquefaction on Spectral Acceleration. *Journal of Geotechnical and Geoenvironmental Engineering* 131: 811–25. https://doi.org/10.1061/(ASCE)1090-0241(2005)131:7(811).

[14] Hashash, Y.M.A., M.I. Musgrove, J.A. Harmon, O. Ilhan, G. Xing, O. Numanoglu, D. Groholski, C.A. Phillips, and D. Park. 2020. DEEPSOIL V7.0, User Manual. Board of Trustees of the University of Illinois at Urbana-Champaign. Urbana, IL.

[15] Sieh, K., and D. Natawidjaja. 2000. Neotectonics of the Sumatran fault, Indonesia. *Journal of Geophysical Research* 105: 28 295-28 326. doi:10.1029/2000JB900120.

[16] McCaffrey, R. 2009. The Tectonic Framework of the Sumatran Subduction Zone. *Annual Review of Earth and Planetary Sciences* 37: 345–66. https://doi.org/10.1146/annurev.earth.031208.100212.

[17] Naryanto, H.N. 1997. Kegempaan di Daerah Sumarta. *Alami* 2.

[18] United States Geological Survey (USGS). 2022.

[19] Green, R.A., and J.J. Bommer. What Is the Smallest Earthquake Magnitude That Needs to Be Considered in Assessing Liquefaction Hazard? *Earthquake Spectra* 35: 1441–64. https://doi.org/10.1193/032218EQS064M.

[20] Jalil, A., T.F. Fathani, I. Satyarno, and W. Wilopo. 2020. A Study on the Liquefaction Potential in Banda Aceh City after the 2004 Sumatra Earthquake. *International Journal of GEOMATE* 18: 147–155. https://doi.org/10.21660/2020.65.94557.

[21] Ministry of Public Works and Housing. 2022. Earthquake Disaggregation Book 2022 For Planning and Evaluation of Earthquake Resistant Infrastructure.

[22] Kempton, J.J., and J.P. Stewart. 2006. Prediction Equations for Significant Duration of Earthquake Ground Motions Considering Site and Near-Source Effects. *Earthquake Spectra* 22: 985–1013.

[23] Pacific Earthquake Engineering Research Center. NGA-West2 – Shallow Crustal Earthquakes in Active Tectonic Regimes.

[24] Rezaeian, S., P.S. Zhong, H. Hartzell, and F. Zareian. 2015. Validation of Simulated Earthquake Ground Motions Based on Evolution of Intensity and Frequency Content. *Bull. Seismol. Soc. Am* 105.

[25] Karina P. A., S. Ismanto, A. Saputra. 2023. Liquefaction Potential Evaluation In Toba Crater Indonesia. Geomate, vol. 25, no. 110, Sep. 2023, doi: 10.21660/2023.110.3990.

[26] Groholski, D. 2015. Evaluation of 1-D Non-linear Site Response Analysis using a General Quadratic/Hyperbolic Strength-Controlled Constitutive Model.

[27] Brandenberg, S.J., N. Bellana, and T. Shantz. 2010. Shear wave velocity as function of standard penetration test resistance and vertical effective stress at California bridge sites. *Soil Dynamics and Earthquake Engineering* 30: 1026–1035. https://doi.org/10.1016/j.soildyn.2010.04.014.

[28] Darendeli, M.B. 2001. Development of a New Family of Normalized Modulus Reduction and Material Damping Curves.

[29] Sonmez, H., and C. Gokceoglu. 2005. A Liquefaction Severity Index Suggested to Engineering Practice. *Environmental Geology* 48: 81–91. DOI 10.1007/s00254-005-1263-9

[30] Idriss, I.M., and R.W. Boulanger. 2008. Soil Liquefaction During Earthquakes. Machinery and Production Engineering. https://doi.org/10.1177/136218079700300202.

[31] Idriss, I.M., and R.W. Boulanger. *CPT and SPT Based Liquefaction Triggering Procedures*. Center for Geotechnical Modeling.

[32] Iwasaki, T., T. Arakawa, and K. Tokida. 1984. Simplified Procedures for Assessing Soil Liquefaction during Earthquakes. *International Journal of Soil Dynamics and Earthquake Engineering* 3: 49–58. https://doi.org/10.1016/0261-7277(84)90027-5.

[33] Sonmez, H. 2003. Modification of the Liquefaction Potential Index and Liquefaction Susceptibility Mapping for a Liquefaction-Prone Area (Inegol,Turkey. *Environmental Geology* 44: 862–71. https://doi.org/10.1007/s00254-003-0831-0.

[34] Fathani, T.F., A.D. Adi, S. Pramumijoyo, and D. Karnawati. 2008. The Determination of Peak Ground Acceleration at Bantul Regency, Yogyakarta Province, Indonesia. *Yogyakarta Earthq*: 1–15.

[35] Mase, L.Z., S. Likitlersuang, S. Soralump, and T. Tobita. 2015. Empirical Study of Liquefaction Potential in Chiang Rai Province in North of Thailand. https://doi.org/10.13140/RG.2.1.1706.1840.

[36] Youd, T.L., I.M. Idriss, R.D. Andrus, I. Arango, G. Castro, J.T. Christian, R. Dobry, et al. 2001. Liquefaction Resistance of Soils: Summary Report from the 1996 NCEER and 1998 NCEER/NSF Workshops on Evaluation of Liquefaction Resistance of Soils. *Journal of Geotechnical and Geoenvironmental Engineering* 127: 817–33. https://doi.org/10.1061/(ASCE)1090-0241(2001)127:10(817).

[37] Hakam, A., and E. Suhelmidawati. 2013. Liquefaction Due to September 30, 2009 Earthquake in Padang. *Procedia Engineering* 54: 140–46. https://doi.org/10.1016/j.proeng.2013.03.013.

[38] Youd, T.L., J.C. Tinsley, D.M. Perkins, E.J. King, and R.F. Preston. 1979. Liquefaction Potensial Map of. San Fernando Valley, California.

[39] Seed, H.B., K. Tokimatsu, L.F. Harder, and R.M. Chung. 1985. of SPT procedures in soil liquefaction resistance evaluations. *Journal of Geotechnical Engineering* 111: 1425–1444. https://doi.org/10.1061/(ASCE)0733-9410(1985)111:12(1425).

[40] Bawankule, M., & S. N. Pawar. 2022. Evaluation of Liquefaction Potential of Nagpur Region Using SPT Data: Field Assessment. IOP Conference Series: Earth and Environmental Science, 1086(1): 012021. https://doi.org/10.1088/1755-1315/1086/1/012021